

Altermagnetism-driven FFLO superconductivity in finite-filling 2D lattices

Xia-Ji Liu^{1,*} and Hui Hu¹

¹Centre for Quantum Technology Theory, Swinburne University of Technology, Melbourne 3122, Australia

(Dated: January 13, 2026)

We systematically investigate the emergence of finite-momentum Fulde-Ferrell-Larkin-Ovchinnikov (FFLO) superconductivity in a square lattice Hubbard model with finite filling, driven by either d_{xy} -wave or $d_{x^2-y^2}$ -wave altermagnetic order in the presence of on-site s -wave attractive interactions. Our study combines mean-field calculation in the superconducting phase with pairing instability analysis of the normal state, incorporating the next-nearest-neighbor hopping in the single-particle dispersion relation. We demonstrate that the two types of altermagnetism have markedly different impacts on the stabilization of FFLO states. Specifically, d_{xy} -wave altermagnetism supports FFLO superconductivity over a broad parameter regime at low fillings, whereas $d_{x^2-y^2}$ -wave altermagnetism only induces FFLO pairing in a narrow range at high fillings. Furthermore, we find that the presence of a Van Hove singularity in the density of states tends to suppress FFLO superconductivity. These findings may provide guidance for experimental exploration of altermagnetism-induced FFLO states in real materials with more complex electronic structures.

I. INTRODUCTION

Altermagnetism is a newly-identified type of magnetic ordering in crystalline materials [1–3], distinct from the two long-known classes of ferromagnetism and antiferromagnetism. In altermagnetic materials (commonly called altermagnets), despite the total magnetic moment adding up to zero (as in antiferromagnets), the electronic bands exhibit a significant spin splitting (a trait of ferromagnets) [4–12]. This unique combination makes altermagnets compelling for ultrafast spintronics applications with improved scalability. The presence of spin-splitting is especially intriguing and opens up a new frontier in exploring novel quantum many-body phenomena in condensed matter physics [2, 3].

In this context, the prospect of unconventional superconductivity driven by altermagnetism has garnered increasing attention [3, 13–15]. In particular, Zhang, Hu and Neupert predicted the possibility of finite-momentum Cooper pairing by modeling altermagnets in proximity to conventional s -wave superconductors [16]. That intriguing proposal opens the way for spatially inhomogeneous Fulde–Ferrell–Larkin–Ovchinnikov (FFLO) state superconductivity [17–27] in altermagnetic metals [28–36]. Indeed, earlier work on quantum spin-nematic phases established that a d -wave spin-splitting band structure can give rise to FFLO states in the presence of attractive d -wave interactions [37]. More recently, Chakraborty and Black-Schaffer confirmed the emergence of FFLO superconductivity induced by d -wave altermagnetism with d -wave interaction potentials [29]. A subsequent study by Hong, Park and Kim [30] demonstrated that such an FFLO state can also arise under s -wave interactions – challenging the earlier belief that d -wave interactions are essential. That discrepancy has now been resolved through further analytic

and numerical work by Hu and collaborators [34, 36].

It is worth noting that most of the aforementioned theoretical studies on FFLO superconductivity adopted a single-band model of altermagnetism. More realistic modeling that incorporates the sub-lattice degree of freedom was performed by Sumita, Naka and Seo [33]. Based on a Ginzburg–Landau framework, their detailed analysis clearly showed that a phase-modulated (plane-wave-like) Fulde–Ferrell form of the superconducting order parameter is favored when a two-band model for sub-lattices are used, rather than the amplitude-modulated Larkin–Ovchinnikov type or other more complex FFLO configurations [33].

In this work, we would like to revisit altermagnetism-driven FFLO superfluidity in two-dimensional lattices by systematically examining various types of d -wave altermagnetism using more realistic single-particle dispersion relations at different electron filling factors. The motivation for this study is two-fold.

First, previous research has primarily focused on either $d_{x^2-y^2}$ -wave [29] or d_{xy} -wave altermagnetism [30, 34]. While these two types are equivalent in the dilute limit with very low filling, they may exhibit distinct effects on superconducting states at finite or high filling factors. A comparative investigation is therefore essential to clarify their differing roles in inducing FFLO superconductivity. On the other hand, most earlier studies assumed a single-particle dispersion including only the nearest-neighbor hopping. It is thus of interest to explore altermagnetism-driven FFLO superconductivity within more complex and realistic electronic structures, for instance, when next-nearest-neighbor hopping is present. Such modification shifts the Van Hove singularity in the electronic density of states away from half-filling, raising questions about how this singularity influences superconducting behavior [33].

We employ two complementary theoretical approaches to investigate FFLO superconductivity. In the superconducting regime, we explicitly solve the mean-field Bogoliubov–de Gennes equations to determine the finite-

* Corresponding author: xiajiliu@swin.edu.au

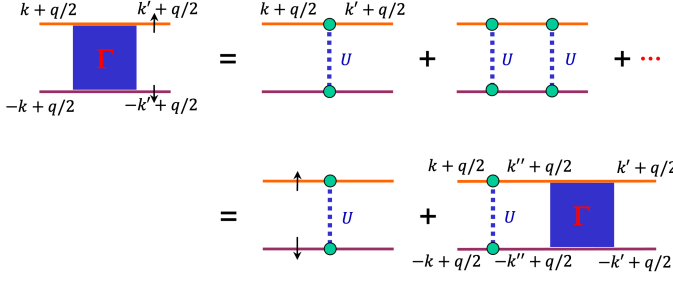


FIG. 1. Diagrammatic representation of the two-particle vertex function $\Gamma(\mathbf{k}, \mathbf{k}'; \mathbf{q}, \omega)$, within the ladder approximation.

momentum order parameter. In the normal state with relatively strong altermagnetic coupling, we analyze the onset of finite-momentum pairing instability using the well-established Thouless criterion. Together, these approaches provide a comprehensive phase diagram of the superconducting states as functions of the filling factor and altermagnetic coupling strength.

The remainder of this paper is organized as follows. In Sec. II, we introduce the model Hamiltonian that describes d -wave altermagnetic metals in two-dimensional lattices. Section III outlines the solution of this model using standard mean-field approaches. In Sec. IV, we construct and analyze the phase diagram for both $d_{x^2-y^2}$ -wave and d_{xy} -wave altermagnetism. Finally, Sec. V provides concluding remarks. In Appendix A, we consider the temperature effect. In Appendix B, we present additional results at low filling factors, explicitly demonstrating the equivalence between $d_{x^2-y^2}$ -wave and d_{xy} -wave altermagnetism in driving FFLO superconductivity in the dilute limit.

II. MODEL HAMILTONIAN

We describe a 2D altermagnetic metal on square lattices with an area \mathcal{S} , by using the effective single-band Hamiltonian, $\mathcal{H} = \mathcal{H}_0 + \mathcal{H}_{\text{int}}$, where

$$\mathcal{H}_0 = \sum_{\mathbf{k}\sigma} [\xi_{\mathbf{k}} + s(\sigma) J_{\mathbf{k}}] c_{\mathbf{k}\sigma}^{\dagger} c_{\mathbf{k}\sigma}, \quad (1)$$

$$\mathcal{H}_{\text{int}} = \frac{U}{\mathcal{S}} \sum_{\mathbf{k}, \mathbf{k}', \mathbf{q}} c_{\mathbf{k}+\frac{\mathbf{q}}{2}\uparrow}^{\dagger} c_{-\mathbf{k}+\frac{\mathbf{q}}{2}\downarrow}^{\dagger} c_{-\mathbf{k}'+\frac{\mathbf{q}}{2}\downarrow} c_{\mathbf{k}'+\frac{\mathbf{q}}{2}\uparrow} \quad (2)$$

are the non-interacting Hamiltonian and the interacting Hamiltonian, respectively, and $c_{\mathbf{k}\sigma}^{\dagger}$ ($c_{\mathbf{k}\sigma}$) are the creation (annihilation) field operators. We consider the spin-independent single-particle dispersion relation [38],

$$\xi_{\mathbf{k}} = -2t(\cos k_x + \cos k_y) - 4t' \cos k_x \cos k_y - \mu, \quad (3)$$

where t and t' are the nearest-neighbor and the next-to-nearest-neighbor hopping strengths, and μ is the chemical potential that controls the lattice filling factor. The presence of the altermagnetism introduces a spin-dependent band-splitting, $s(\uparrow)J_{\mathbf{k}} = +J_{\mathbf{k}}$ and $s(\downarrow)J_{\mathbf{k}} = -J_{\mathbf{k}}$, for spin-up and spin-down electrons, respectively. We include the two forms of the d -wave altermagnetism,

$$J_{\mathbf{k}} = -\lambda \sin k_x \sin k_y \quad (4)$$

for the d_{xy} -wave type [30] and

$$J_{\mathbf{k}} = -\frac{t_{\text{am}}}{2} (\cos k_x - \cos k_y) \quad (5)$$

for the $d_{x^2-y^2}$ -wave type [29], respectively. For simplicity, here we consider the on-site attraction $U < 0$ only, which gives rise to the spin-singlet pairing between two electrons with unlike spins.

III. THEORETICAL FRAMEWORK

We now present the theoretical approaches used to study the FFLO state, both when the system is in the normal (non-superconducting) phase, and when it is already superconducting.

A. Thouless criterion for the pairing instability

In the normal phase, we examine whether the system becomes unstable to pair formation for given parameters, such as temperature T , interaction strength U , and the altermagnetic coupling constant λ or t_{am} . A convenient way to check this is via the Thouless criterion, which states that the instability sets in when the inverse two-particle vertex function satisfies [39, 40],

$$\max_{\{\mathbf{q}\}} \Gamma^{-1}(\mathbf{q}, \omega = 0) = 0. \quad (6)$$

In the case that the maximum of the inverse vertex function occurs at a nonzero momentum $\mathbf{q} \neq 0$, the normal state is unstable towards the formation of an inhomogeneous finite-momentum FFLO state.

In this work, we use the standard non-self-consistent T -matrix approach [39, 40]. By summing all the ladder diagrams illustrated in Fig. 1, we may formally write the equation satisfied by the approximate vertex function,

$$\Gamma(\mathbf{k}, \mathbf{k}'; \mathbf{q}, \omega) = U - \sum_{k''} U G_{0\uparrow} \left(k'' + \frac{q}{2} \right) G_{0\downarrow} \left(-k'' + \frac{q}{2} \right) \Gamma(\mathbf{k}'', \mathbf{k}'; \mathbf{q}, \omega), \quad (7)$$

where we have introduced the four-momenta $q = \{\mathbf{q}, i\nu_n \rightarrow \omega + i0^+\}$ and $k'' = \{\mathbf{k}'', i\omega_m\}$, with the bosonic and fermionic Matsubara frequencies $\nu_n = 2\pi nT$ and $\omega_m = 2\pi(m + 1/2)T$ ($n, m \in \mathbb{Z}$), respectively. We have also abbreviated the summation $\sum_{k''} \equiv (k_B T / \mathcal{S}) \sum_{\omega_m} \sum_{\mathbf{k}''}$. It is readily seen that the two-particle vertex function is independent on \mathbf{k} and \mathbf{k}' , due to the contact-like on-site interaction U . The summation over the fermionic Matsubara frequency ω_m can be easily carried out, and we obtain,

$$\Gamma^{-1}(\mathbf{q}, \omega) = \frac{1}{U} + \frac{1}{\mathcal{S}} \sum_{\mathbf{k}''} \frac{\left[n_F\left(\xi_{\frac{\mathbf{q}}{2} + \mathbf{k}''\uparrow}\right) + n_F\left(\xi_{\frac{\mathbf{q}}{2} - \mathbf{k}''\uparrow}\right) - 1 \right]}{\omega^+ - \left(\xi_{\frac{\mathbf{q}}{2} + \mathbf{k}''\uparrow} + \xi_{\frac{\mathbf{q}}{2} - \mathbf{k}''\uparrow}\right)}, \quad (8)$$

where $\xi_{\mathbf{k}\uparrow} = \xi_{\mathbf{k}} + J_{\mathbf{k}}$ and $\xi_{\mathbf{k}\downarrow} = \xi_{\mathbf{k}} - J_{\mathbf{k}}$, and $n_F(x) \equiv 1/[e^{x/(k_B T)} + 1]$ is the Fermi-Dirac distribution function.

We perform a numerical integration of the momentum \mathbf{k}'' in Eq. (8) across the first Brillouin zone of the square lattice, using a small imaginary broadening $\eta \sim 0.02t$. The resulting numerical precision of the inverse vertex function can be roughly estimated by verifying that the identity

$$\text{Im}\Gamma^{-1}(\mathbf{q}, \omega = 0) = 0 \quad (9)$$

is satisfied within some tolerance.

B. Mean-field theory

In the superconducting phase, we assume a (real) order parameter $\Delta = -(U/\mathcal{S}) \sum_{\mathbf{k}} \langle c_{-\mathbf{k}+\mathbf{q}/2\downarrow} c_{\mathbf{k}+\mathbf{q}/2\uparrow} \rangle$ in momentum space to search for the inhomogeneous superconductivity at a finite-momentum \mathbf{q} [21, 34], whose direction is determined by the type of altermagnetism. In real space, this order parameter corresponds to a phase-modulated form, $\Delta(\mathbf{x}) = \Delta e^{i\mathbf{q}\cdot\mathbf{x}}$. By taking the mean-field decoupling of the interaction Hamiltonian,

$$\mathcal{H}_{\text{int}} \simeq - \sum_{\mathbf{k}} \left[\Delta c_{\mathbf{k}+\frac{\mathbf{q}}{2}\uparrow}^\dagger c_{-\mathbf{k}+\frac{\mathbf{q}}{2}\downarrow}^\dagger + \text{H.c.} \right] - \frac{\Delta^2}{U} \mathcal{S}. \quad (10)$$

we end up with a bilinear pairing Hamiltonian,

$$\begin{aligned} \mathcal{H} = & \sum_{\mathbf{k}} \left[\xi_{\mathbf{k}+\frac{\mathbf{q}}{2}\uparrow} c_{\mathbf{k}+\frac{\mathbf{q}}{2}\uparrow}^\dagger c_{\mathbf{k}+\frac{\mathbf{q}}{2}\uparrow} + \xi_{\mathbf{k}-\frac{\mathbf{q}}{2}\downarrow} c_{-\mathbf{k}+\frac{\mathbf{q}}{2}\downarrow}^\dagger c_{-\mathbf{k}+\frac{\mathbf{q}}{2}\downarrow} \right] \\ & - \sum_{\mathbf{k}} \left[\Delta c_{\mathbf{k}+\frac{\mathbf{q}}{2}\uparrow}^\dagger c_{-\mathbf{k}+\frac{\mathbf{q}}{2}\downarrow}^\dagger + \text{H.c.} \right] - \frac{\Delta^2}{U} \mathcal{S}, \end{aligned} \quad (11)$$

which can be solved by using the standard Bogoliubov transformation, with the introduction of the Nambu spinor,

$$\Psi_{\mathbf{k}} = \begin{bmatrix} c_{\mathbf{k}+\frac{\mathbf{q}}{2}\uparrow} \\ c_{-\mathbf{k}+\frac{\mathbf{q}}{2}\downarrow}^\dagger \end{bmatrix}. \quad (12)$$

More explicitly, we rewrite the pairing Hamiltonian in the form,

$$\mathcal{H} = \sum_{\mathbf{k}} \Psi_{\mathbf{k}}^\dagger \begin{bmatrix} \xi_{\mathbf{k}+\frac{\mathbf{q}}{2}\uparrow} & -\Delta \\ -\Delta & \xi_{\mathbf{k}-\frac{\mathbf{q}}{2}\downarrow} \end{bmatrix} \Psi_{\mathbf{k}} - \frac{\Delta^2}{U} \mathcal{S} + \sum_{\mathbf{k}} \xi_{\mathbf{k}-\frac{\mathbf{q}}{2}\downarrow}. \quad (13)$$

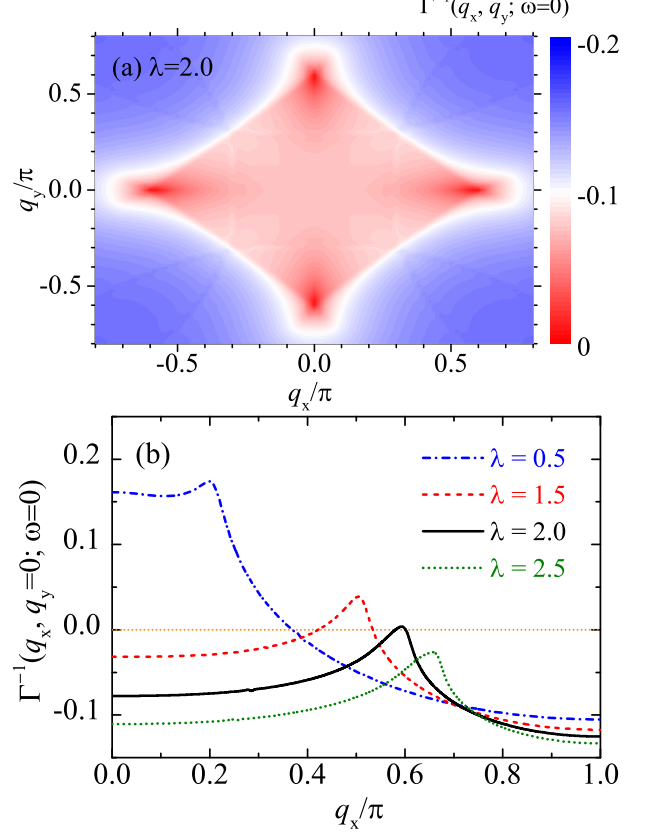


FIG. 2. (a) The inverse vertex function at zero frequency $\Gamma^{-1}(\mathbf{q}, \omega = 0)$, in units of t^{-1} , in the q_x - q_y plane at the altermagnetic coupling $\lambda = 2t$. The inverse vertex function reaches maximum at $(q_x, q_y) = (\pm q, 0)$ or $(0, \pm q)$, where $q = |\mathbf{q}|$. (b) $\Gamma^{-1}(q_x, q_y = 0; \omega = 0)$ at different altermagnetic couplings λ as indicated. Here, we consider the d_{xy} -wave altermagnetism and take an attraction strength $U = -3t$ at the filling factor $\nu = 1.0$. We have taken a negligible temperature $T = 0.01t$ to smooth the sharp Fermi surface and to increase numerical accuracy.

The diagonalization of the two by two matrix leads to two Bogoliubov excitation spectra [30], indexed by $\eta = \pm$:

$$E_{\mathbf{k}\pm} = \sqrt{A_{\mathbf{k}}^2 + \Delta^2} \pm B_{\mathbf{k}}, \quad (14)$$

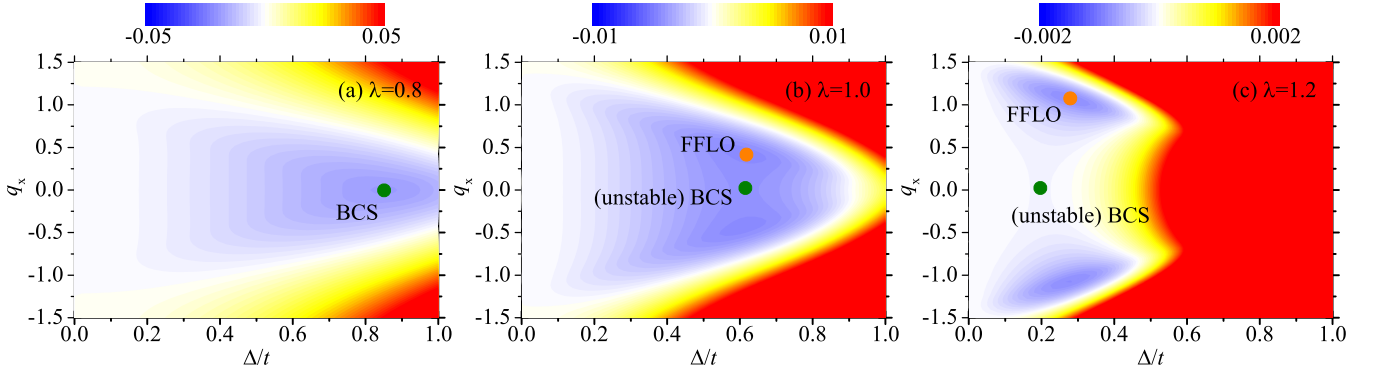


FIG. 3. The contour plots of the thermodynamic potential $(\Omega - \Omega_0)/(\nu t)$, as functions of the pairing amplitude Δ and the FFLO momentum q_x , at three altermagnetic coupling strengths: $\lambda = 0.8t$ (a), $\lambda = 1.0t$ (b) and $\lambda = 1.2t$ (c). The chemical potential in each plot is, $\mu = 2.05t$ (a), $\mu = 1.98t$ (b) and $\mu = 1.91t$ (c). The green dots indicate the stable or unstable BCS states, while the orange dots highlight the FFLO state. Here, we consider the d_{xy} -wave altermagnetism and take an attraction strength $U = -3t$ at the filling factor $\nu = 1.0$.

where

$$A_{\mathbf{k}} \equiv \frac{1}{2} \left(\xi_{\frac{\mathbf{q}}{2}+\mathbf{k}} + \xi_{\frac{\mathbf{q}}{2}-\mathbf{k}} + J_{\frac{\mathbf{q}}{2}+\mathbf{k}} - J_{\frac{\mathbf{q}}{2}-\mathbf{k}} \right), \quad (15)$$

$$B_{\mathbf{k}} \equiv \frac{1}{2} \left(\xi_{\frac{\mathbf{q}}{2}+\mathbf{k}} - \xi_{\frac{\mathbf{q}}{2}-\mathbf{k}} + J_{\frac{\mathbf{q}}{2}+\mathbf{k}} + J_{\frac{\mathbf{q}}{2}-\mathbf{k}} \right). \quad (16)$$

The corresponding grand thermodynamic potential at finite temperature T takes the form,

$$\Omega = -\frac{\Delta^2}{U} \mathcal{S} + \mathcal{E}_0 - k_B T \sum_{\mathbf{k}, \eta=\pm} \ln \left(1 + e^{-\frac{E_{\mathbf{k}\eta}}{k_B T}} \right), \quad (17)$$

where

$$\mathcal{E}_0 \equiv \sum_{\mathbf{k}} \left(\xi_{\frac{\mathbf{q}}{2}-\mathbf{k}\downarrow} - E_{\mathbf{k}-} \right) = \sum_{\mathbf{k}} \left(A_{\mathbf{k}} - \sqrt{A_{\mathbf{k}}^2 + \Delta^2} \right) \quad (18)$$

denotes the energy offset that arises from performing the Bogoliubov transformation - in the process of expressing the quasiparticle field operators in proper order, and the last term is the usual free-fermion contribution from Bogoliubov quasiparticles. For fixed chemical potential μ (measured from the bottom of the single-particle dispersion relation $\xi_{\mathbf{k}}$) and temperature T , the two independent parameters are the order parameter Δ and the FFLO momentum q . Their equilibrium values are determined by minimizing the thermodynamic potential, i.e.,

$$\frac{\partial \Omega}{\partial \Delta} = 0, \quad (19)$$

$$\frac{\partial \Omega}{\partial q} = 0. \quad (20)$$

Finally, the chemical potential is adjusted so that the number equation,

$$\nu = -\partial \Omega / \partial \mu, \quad (21)$$

is satisfied for the given filling factor ν .

IV. RESULTS AND DISCUSSIONS

Throughout this work, we take the next-to-nearest-neighbor hopping strength $t' = -0.35t$ [38], as a typical value for the candidate altermagnetic materials. This nonzero hopping strength t' breaks the particle-hole symmetry at the half-filling $\nu = 1$ and moves the position of the Van Hove singularity to a smaller filling factor $\nu_{\text{VH}} \simeq 0.66$ [38]. We also take an on-site attraction $U = -3t$ and an essentially zero temperature $T = 0.01t$, unless specified otherwise. In the following, we discuss separately the two cases of the d_{xy} - and $d_{x^2-y^2}$ -wave altermagnetism.

A. d_{xy} -wave altermagnetism

In Fig. 2(a), we report a contour map of the zero-frequency inverse vertex function $\Gamma^{-1}(\mathbf{q}, \omega = 0)$ as a function of the pairing momentum components q_x and q_y , for d_{xy} -wave altermagnetism with coupling strength $\lambda = 2t$ at half-filling ($\nu = 1$). It is immediately evident that the maximum of Γ^{-1} lies along either the q_x -axis or the q_y -axis [30]. Importantly, this behavior remains robust across other filling factors ν and different altermagnetic coupling constants λ . As a consequence, in our numerical calculations we may without loss of generality take $\mathbf{q} = q_x \mathbf{e}_x$ for d_{xy} -wave altermagnetism. Then, in Fig. 2(b) we plot the dependence of $\Gamma^{-1}(\mathbf{q}, \omega = 0)$ on q_x for several values of λ . According to the Thouless criterion, a non-negative value of Γ^{-1} signals that the system enters a superconducting phase. We observe that the transition to this superconducting phase sets in around $\lambda \simeq 2t$, where the nonzero optimal pairing momentum $q_{x,\text{max}} \simeq 0.6\pi$ indicates that the emergent superconducting state is spatially inhomogeneous.

To analyze the symmetry-breaking phases in the superconducting domain, we apply the Bogoliubov mean-

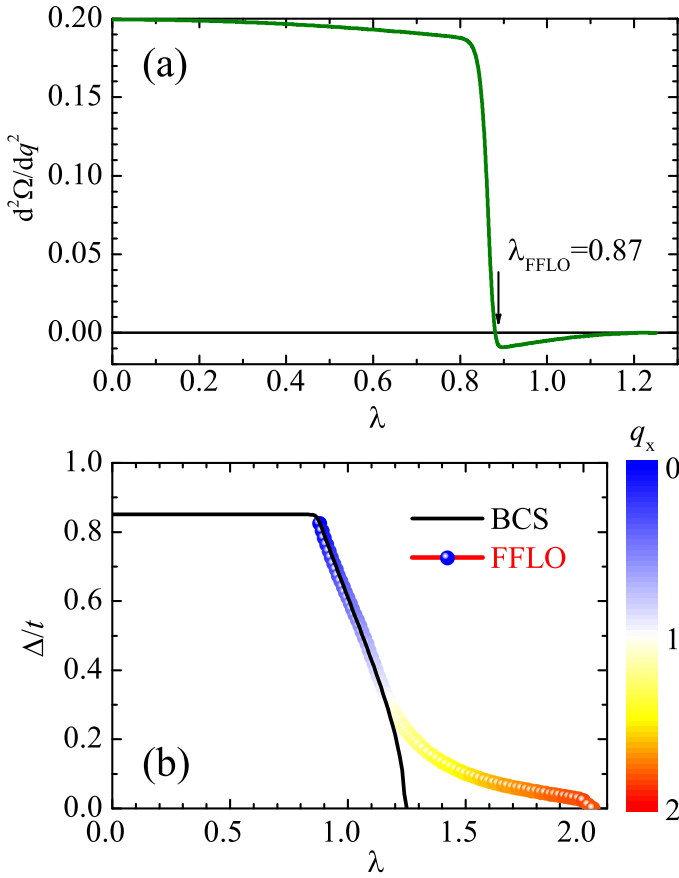


FIG. 4. (a) The second derivative $\partial^2\Omega/\partial q_x^2$ of the BCS state as a function of λ . It becomes negative at $\lambda_{\text{FFLO}} \simeq 0.87t$, where the FFLO state starts to emerge. (b) The pairing gaps of the BCS state (solid line) and of the FFLO state (colored dots) as a function of the altermagnetic coupling strength λ . The color of the dots shows the values of the FF momentum q_x , following the color map. Here, we consider the d_{xy} -wave altermagnetism and take an attraction strength $U = -3t$ at the filling factor $\nu = 1.0$.

field approach. In Fig. 3, we show the contour plots of the thermodynamic potential Ω versus the pairing amplitude Δ and the FF momentum q_x , for various values of the altermagnetic coupling strengths, taking the non-interacting thermodynamic potential Ω_0 as a reference point. For weak altermagnetic coupling (see Fig. 3(a)), the potential landscape exhibits a single global minimum, corresponding to the conventional uniform BCS state with $q_x = 0$. As the altermagnetic coupling strength grows (Fig. 3(b)), the BCS minimum becomes unstable (i.e., turning into a saddle point), while a new global minimum emerges at nonzero $\pm q_x$, indicating the onset of an inhomogeneous FFLO phase. By further increasing λ (Fig. 3(c)), the FFLO minimum moves well away from the now-unstable BCS saddle point and becomes increasingly pronounced.

The above instability of the uniform BCS state toward an inhomogeneous FFLO phase could be tracked by the

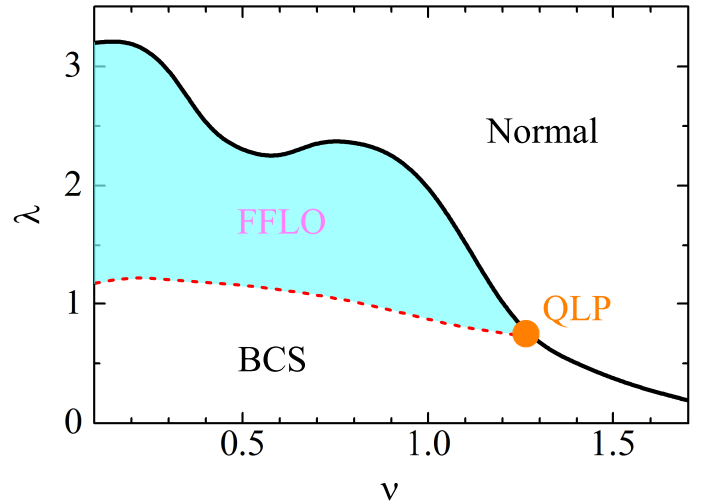


FIG. 5. The phase diagram under the d_{xy} -wave altermagnetism, as functions of the filling factor ν and the altermagnetic coupling strength λ . The transition from the BCS state to the FFLO state is shown by the red dashed line, while the transition from the FFLO state to the normal state is shown by the black solid line. The three phases meet at a quantum Lifshitz point, as highlighted by an orange dot. Here, we take an attraction strength $U = -3t$.

phase stiffness: a negative stiffness under a phase twist (i.e., $\rho_s \propto \partial\Omega^2/\partial q^2 < 0$) signals that the uniform state is unstable to finite-momentum pairing. In Fig. 4(a), we present the second derivative $\partial^2\Omega/\partial q_x^2$ with increasing the altermagnetic coupling. We find that this curvature decreases sharply once $\lambda > 0.8t$ and becomes negative around a critical coupling $\lambda_{\text{FFLO}} \simeq 0.87$, indicating the loss of stability of the uniform phase. Beyond this threshold, the pairing amplitude of the (meta-stable) BCS solution drops quickly and vanishes near $\lambda \sim 1.25t$, as seen in Fig. 4(b). The stable FFLO phase has a relatively small pairing amplitude, but it persists up to $\lambda_c \sim 2t$, thus providing a relatively wide parameter range in which the FFLO state appears.

We repeat the numerical analysis at different filling factors to construct a superconducting phase diagram under d_{xy} -wave altermagnetism, as reported in Fig. 5. In this diagram, the boundary marking the transition from the uniform BCS state to the FFLO phase (λ_{FFLO}) is indicated by the red dashed line, and the line marking the transition from the FFLO phase to the normal state (λ_c) is shown as a solid black curve. As the filling factor increases, the threshold coupling λ_{FFLO} steadily decreases, while the critical coupling λ_c exhibits a non-monotonic dependence on filling. Near $\nu \simeq 0.6$, the parameter range supporting the FFLO phase narrows significantly, a feature that might be associated with proximity to the Van Hove singularity in the density of states. The FFLO window eventually disappears at large filling (i.e., $\nu \simeq 1.25$). As a result, the phase diagram reveals a quantum Lifshitz point at which the BCS, FFLO, and normal phases

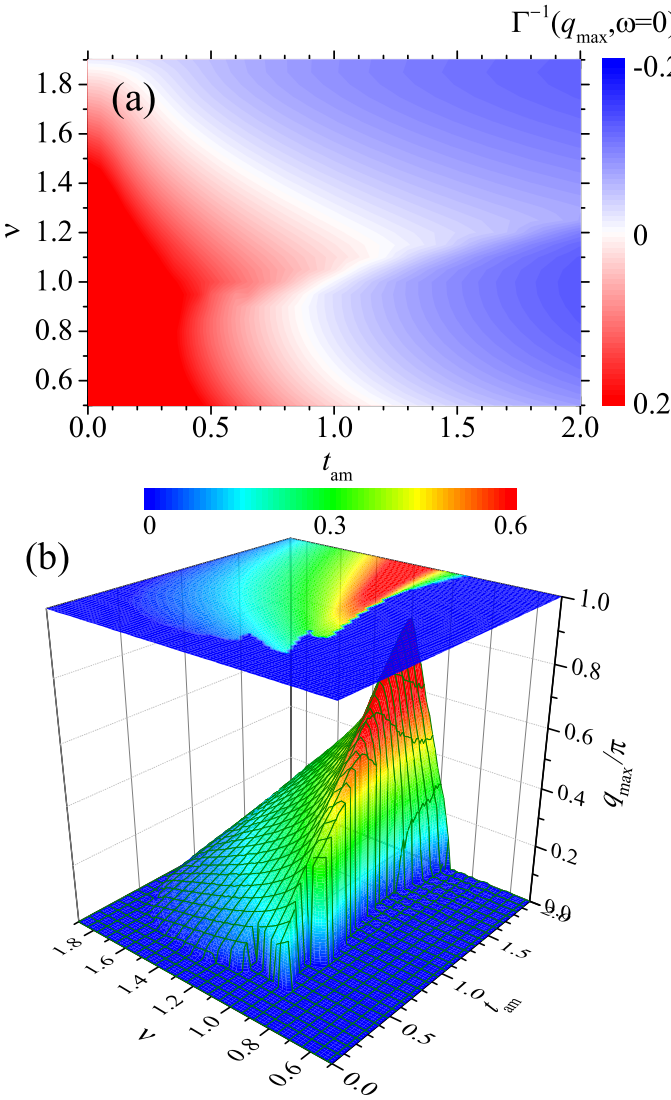


FIG. 6. (a) The maximum of the inverse vertex function $\Gamma^{-1}(q_{\max}, \omega = 0)$ and the corresponding pairing momentum q_{\max} (b) as functions of the altermagnetic coupling t_{am} and the filling factor ν . The contour line in white color in (a) indicates the Thouless criterion $\Gamma^{-1} = 0$ that separates the superconducting phase from the normal state. Here, we consider the $d_{x^2-y^2}$ -wave altermagnetism and take an attraction strength $U = -3t$. In this case, the FFLO pairing instability occurs at the filling factor $\nu \gtrsim 1$ only.

converge, marking a multi-critical point where all three phases meet [41, 42].

B. $d_{x^2-y^2}$ -wave altermagnetism

We now examine superconductivity in the presence of $d_{x^2-y^2}$ -wave altermagnetism. In this situation, the inverse vertex function $\Gamma^{-1}(\mathbf{q}, \omega = 0)$ attains its maximum along the diagonal (or off-diagonal) directions, namely at $q_x = \pm q_{\max}/\sqrt{2}$ and $q_y = \pm q_{\max}/\sqrt{2}$. Consequently,

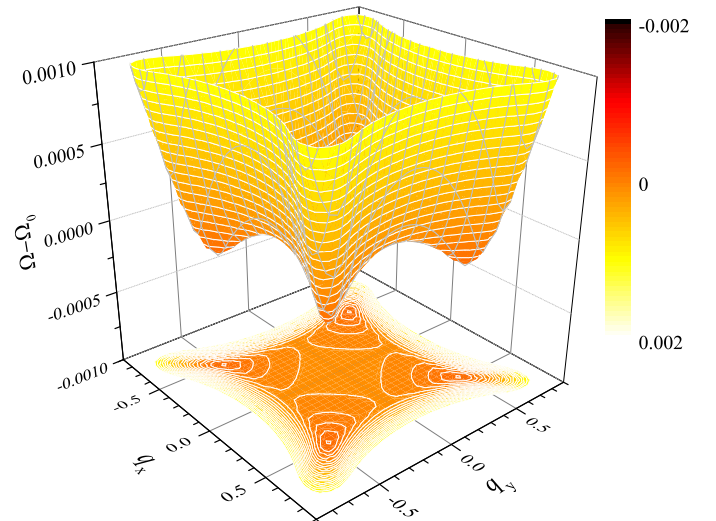


FIG. 7. The landscape of the thermodynamic potential $(\Omega - \Omega_0)/(\nu t)$, as a function of the FFLO momenta q_x and q_y , at the altermagnetic coupling strength $t_{\text{am}} = 0.9t$ and the filling factor $\nu = 1.2$. We have used a pairing gap $\Delta_{\text{FFLO}} = 0.196t$ and a chemical potential $\mu_{\text{FFLO}} = 2.62t$. The thermodynamic potential reaches its minimum at $\mathbf{q} = (q_x, q_y) = (\pm q, \pm q)/\sqrt{2}$, the diagonal or off-diagonal direction. Here, we consider the $d_{x^2-y^2}$ -wave altermagnetism and take an attraction strength $U = -3t$.

in our numerical analysis we take $(q_x, q_y) = (q, q)/\sqrt{2}$ without loss of generality.

In Fig. 6, we present the contour maps of $\Gamma^{-1}(q = q_{\max}, \omega = 0)$ and of q_{\max} as a function of the $d_{x^2-y^2}$ -wave altermagnetic coupling t_{am} and the filling factor ν . According to the Thouless criterion in Eq. (6), the superconducting phase (highlighted in red) is enclosed by the white contour line (see Fig. 6(a)). This boundary exhibits a pronounced, non-monotonic dependence on the filling factor. As before, we observe a suppression of the superconducting region around $\nu \sim 0.8$, which might be related to the appearance of the Van Hove singularity. Remarkably, from Fig. 6(b) we find that a finite-momentum pairing emerges only at sufficiently large filling factors. As the filling factor ν increases from below, q_{\max} abruptly rises from zero to a peak - whose magnitude depends on t_{am} - once $\nu \gtrsim 1$, and then gradually decreases. As a result, we expect that the FFLO phase to be stabilized only at relatively high filling factors, in stark contrast to the behavior found for d_{xy} -wave altermagnetism.

To verify such an anticipation, we carry out the Bogoliubov mean-field calculations in the superconducting states. A representative result is presented in Fig. 7, for the altermagnetic coupling strength $t_{\text{am}} = 0.9t$ and the filling factor $\nu = 1.2$, which yields a pairing amplitude $\Delta_{\text{FFLO}} \simeq 0.196t$. The resulting landscape of the thermodynamic potential $(\Omega - \Omega_0)/(\nu t)$ over the $q_x - q_y$ plane clearly displays four minima located along both the diagonal and off-diagonal directions. This agrees with the

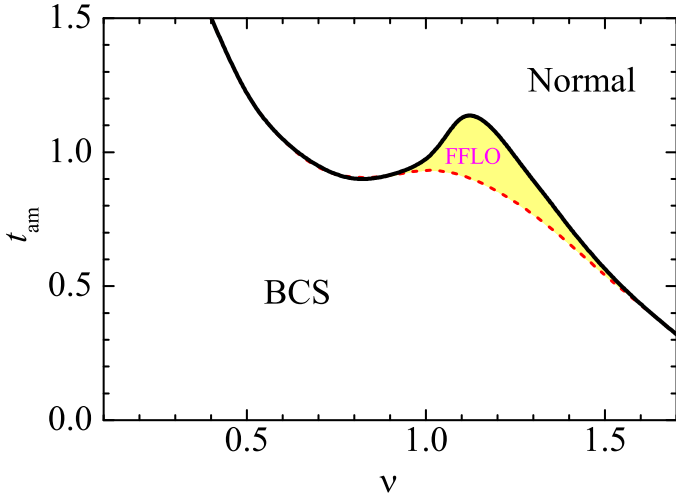


FIG. 8. The phase diagram under the $d_{x^2-y^2}$ -wave altermagnetism, as functions of the filling factor ν and the altermagnetic coupling strength t_{am} . The transition from the BCS state to the FFLO state is shown by the red dashed line, while the transition from the FFLO state to the normal state is shown by the black solid line. Here, we take an attraction strength $U = -3t$.

non-self-consistent T -matrix analysis in the normal state, which indicates that the pairing stability first sets in at $\mathbf{q} = (q_x, q_y) = (\pm q, \pm q)/\sqrt{2}$.

In Fig. 8, we report the phase diagram as a function of the filling factor ν and the $d_{x^2-y^2}$ -wave altermagnetic coupling strength t_{am} . In sharp contrast to the case of d_{xy} -wave altermagnetism, we observe that the parameter window for the existence of the FFLO state is significantly narrowed, indicating that $d_{x^2-y^2}$ -wave altermagnetism is much less effective to stabilizing FFLO superconductivity in lattice systems [29]. For the transition from the superconducting to normal state (i.e., black solid curve in the figure), we still see a suppression of superconductivity around the filling factor $\nu = 0.8$, due to the presence of the Van Hove singularity.

V. CONCLUSIONS AND OUTLOOKS

To conclude, we have investigated the inhomogeneous FFLO state induced by altermagnetism in a two-dimensional metallic system, modeled by electrons on lattices with different filling factors. Pairing instabilities in the normal state were analyzed using a non-self-consistent T -matrix approach, complemented by Bogoliubov mean-field calculations in the superconducting phase. Our systematic investigation have revealed that the parameter regime supporting the FFLO state is highly sensitive to both the type of altermagnetism and the lattice filling. In the case of d_{xy} -wave altermagnetism, the FFLO state is stabilized over a broad range of filling factors. By contrast, for $d_{x^2-y^2}$ -wave altermagnetism, the FFLO phase is much more constrained, appearing

only at high filling and within a narrow parameter window at moderate attractive interactions. This result is consistent with previous studies showing that the FFLO state with s -wave interactions is difficult to realize under $d_{x^2-y^2}$ -wave altermagnetism [29].

A crucial aspect of our study is the inclusion of next-to-nearest-neighbor hopping in the single-particle dispersion, which serves as a simplified yet effective way to emulate the band structure of real materials. This additional hopping term breaks particle-hole symmetry and shifts the location of the Van Hove singularity in the density of states [38]. We have found that the phase boundary associated with the emergence of the FFLO state is strongly influenced by the presence and position of the Van Hove singularity. This pronounced effect is expected to persist even in more realistic two-band descriptions of the single-particle dispersion that explicitly incorporate sub-lattice degrees of freedom [33].

In this work, we have focused on the simplest case of s -wave attractive interactions, which may be mediated by phonons in an altermagnetic metal. However, effective d -wave attractive interactions arising from altermagnetic spin fluctuations are also a plausible pairing mechanism. It would therefore be of considerable interest in future studies to systematically explore altermagnetism-driven FFLO superconductivity in a two-dimensional lattice at finite filling with high-partial-wave pairing interactions.

VI. STATEMENTS AND DECLARATIONS

1. Ethics approval and consent to participate

Not Applicable.

2. Consent for publication

Not Applicable.

3. Availability of data and materials

The data generated during the current study are available from the contributing author upon reasonable request.

4. Competing interests

The authors have no competing interests to declare that are relevant to the content of this article.

5. Funding

This research was supported by the Australian Research Council's (ARC) Discovery Program, Grants Nos.

DP240100248 (X.-J.L.) and DP240101590 (H.H.).

6. Authors' contributions

All the authors equally contributed to all aspects of the manuscript. All the authors read and approved the final manuscript.

7. Acknowledgements

See funding support.

8. Authors' information

Xia-Ji Liu, Centre for Quantum Technology Theory, Swinburne University of Technology, Melbourne 3122, Australia, Email: xiajiliu@swin.edu.au

Hui Hu, Centre for Quantum Technology Theory, Swinburne University of Technology, Melbourne 3122, Australia, Email: hhu@swin.edu.au

Appendix A: The temperature effect

Here, we examine the influence of finite temperature on altermagnetism-driven FFLO superconductivity, focusing on the case of d_{xy} -wave altermagnetism as a representative example. Figures 9(a) and 9(b) display contour plots of $\Gamma^{-1}(q = q_{\max}, \omega = 0)$ and of q_{\max} , respectively, as functions of the altermagnetic coupling strength λ and temperature T . Throughout this analysis, we fix the filling factor at a relatively low value, $\nu = 0.2$. As in previous figures, the superconducting region is highlighted in red, while the transition to the normal state is delineated by the white contour line.

As can be readily seen from Fig. 9(b), the pairing momentum q_{\max} decreases gradually with increasing temperature. Consequently, the parameter regime supporting the uniform BCS state (shown in blue) expands as the temperature rises. Overall, the resulting finite-temperature phase diagram closely resembles that obtained in the presence of an external magnetic field, which likewise induces FFLO superconductivity at sufficiently large field strengths [19, 40]. In particular, we identify a similar Lifshitz point at a finite temperature $T_c \simeq 0.56T_c^{(0)}$, where $T_c^{(0)} \simeq 0.18t$ denotes the BCS transition temperature in the absence of altermagnetism.

Appendix B: Altermagnetism-driven FFLO state in the limit of very low lattice filling

Earlier studies on the altermagnetism-driven FFLO state in 2D lattices have primarily focused on the regime

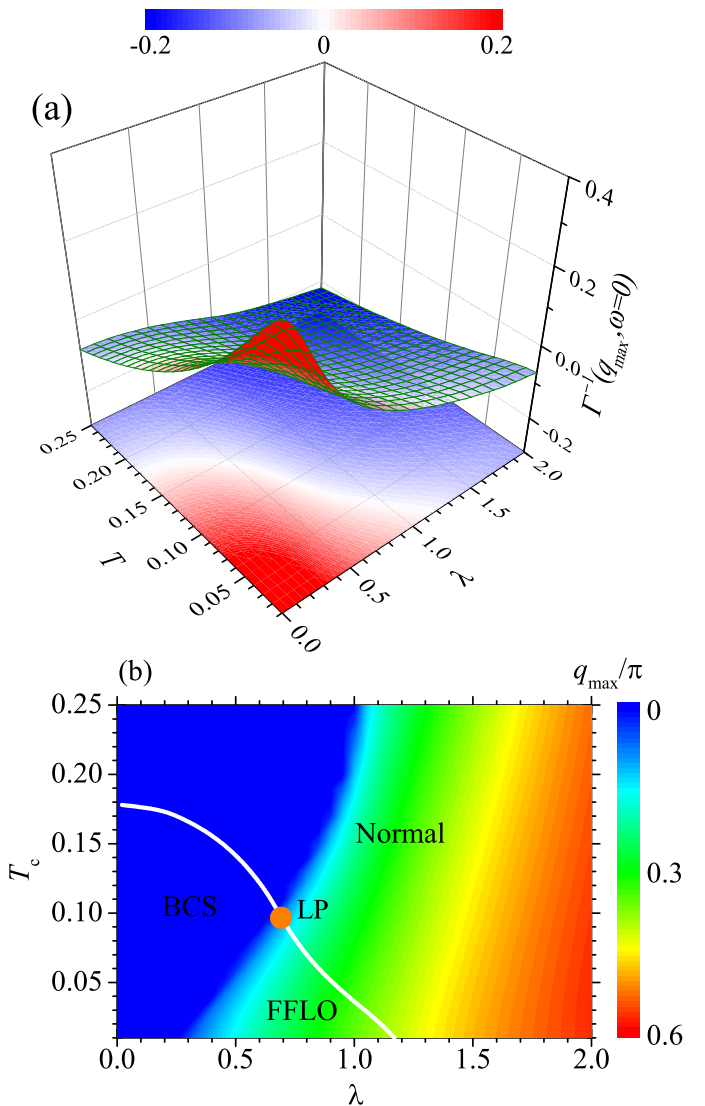


FIG. 9. (a) The maximum of the inverse vertex function $\Gamma^{-1}(q_{\max}, \omega = 0)$ and the corresponding pairing momentum q_{\max} (b) as functions of the altermagnetic coupling λ and the temperature T . The white line in (b) is the critical temperature T_c determined by the Thouless criterion $\Gamma^{-1} = 0$. The orange dot indicates the Lifshitz point at a nonzero temperature. Here, we consider the d_{xy} -wave altermagnetism and take an attraction strength $U = -3t$ at the filling factor $\nu = 0.2$.

of low filling [29, 30, 34], where a continuum model Hamiltonian can be employed as an effective description [34, 36, 37]. In this dilute limit, the specific type of d -wave altermagnetism becomes irrelevant. To illustrate this point, we expand the non-interacting single-particle dispersion relation, including altermagnetic effects, for small k_x and k_y as follows,

$$\xi_{\uparrow, \downarrow}^{(xy)}(\mathbf{k}) = -4t + t(k_x^2 + k_y^2) \pm \lambda k_x k_y \quad (B1)$$

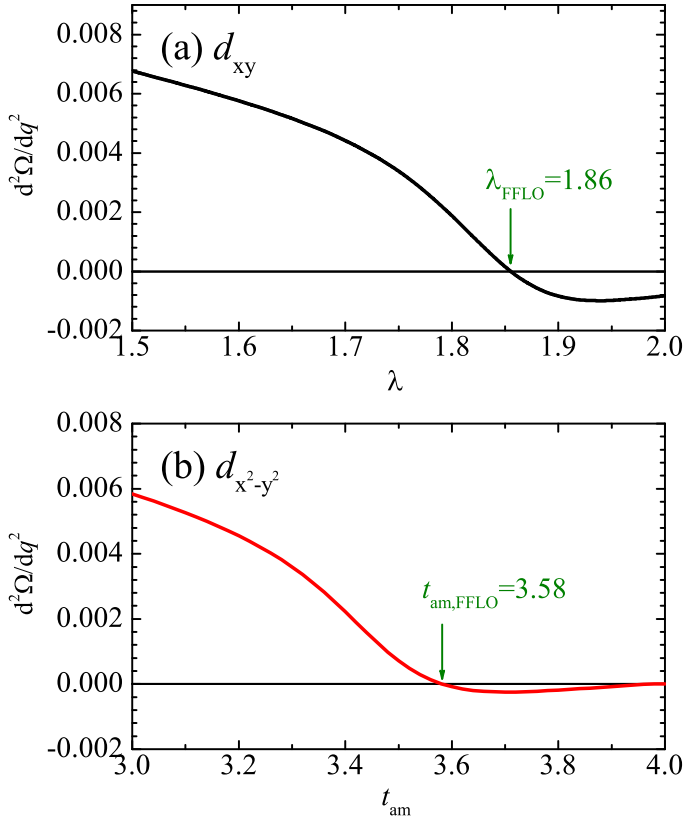


FIG. 10. The second-order derivative $\partial^2\Omega/\partial q_x^2$ of the BCS state, in arbitrary units, as a function of the altermagnetic coupling constant, in the case of d_{xy} -wave altermagnetism (a) or $d_{x^2-y^2}$ -wave altermagnetism (b). Here, we take an attraction strength $U = -4t$ at a small filling factor $\nu = 0.03$. The next-nearest-neighbor hopping strength is set to be zero, $t' = 0$.

for d_{xy} -wave altermagnetism, and

$$\xi_{\uparrow,\downarrow}^{(x^2-y^2)}(\mathbf{k}) = -4t + t(k_x^2 + k_y^2) \pm \frac{t_{\text{am}}}{4}(k_x^2 - k_y^2) \quad (\text{B2})$$

for $d_{x^2-y^2}$ -wave altermagnetism. Here, for simplicity we have set the next-to-nearest-neighbor hopping strength $t' = 0$. It is straightforward to verify that, upon performing a $\pi/4$ rotation in momentum space, i.e., $k_x \rightarrow (k_x + k_y)/\sqrt{2}$ and $k_y \rightarrow (-k_x + k_y)/\sqrt{2}$, the dispersion $\xi_{\uparrow,\downarrow}^{(xy)}(\mathbf{k})$ acquires the same functional form as $\xi_{\uparrow,\downarrow}^{(x^2-y^2)}(\mathbf{k})$, provided that the parameters are identified via,

$$\lambda \longleftrightarrow \frac{t_{\text{am}}}{2}. \quad (\text{B3})$$

In Fig. 10, we present the phase stiffness $\rho_s \sim \partial^2\Omega/\partial q_x^2$ of the uniform BCS state as a function of increasing altermagnetic coupling. Results are shown for the d_{xy} -wave altermagnetism (upper panel) and the $d_{x^2-y^2}$ -wave altermagnetism (lower panel), considering a relatively strong attractive interaction $U = -4t$ and a low filling factor $\nu = 0.03$. Consistent with expectations, the threshold altermagnetic coupling strengths in the two cases approximately obey the relation $\lambda_{\text{FFLO}} = t_{\text{am,FFLO}}/2$.

To conclusively demonstrate that the FFLO state emerges under $d_{x^2-y^2}$ -wave altermagnetism in the dilute limit, we show in Fig. 11 the landscape of the thermodynamic potential $(\Omega - \Omega_0)/(\nu t)$ at a large altermagnetic coupling strength $t_{\text{am}} = 3.7t$. The FFLO phase is clearly identified as the global minimum of the thermodynamic potential landscape.

[1] L. Šmejkal, J. Sinova, and T. Jungwirth, Emerging Research Landscape of Altermagnetism, *Phys. Rev. X* **12**, 040501 (2022).

[2] T. Jungwirth, R. M. Fernandes, E. Fradkin, A. H. MacDonald, J. Sinova, and L. Šmejkal, Altermagnetism: an unconventional spin-ordered phase of matter, *Newton* **1**, 100162 (2025).

[3] Z. Liu, H. Hu, and X.-J. Liu, Altermagnetism and superconductivity: A short historical review, arXiv:2510.09170 (2025).

[4] Y. Noda, K. Ohno, and S. Nakamura, Momentum-dependent band spin splitting in semiconducting MnO₂: a density functional calculation, *Phys. Chem. Chem. Phys.* **18**, 13294 (2016).

[5] M. Naka, S. Hayami, H. Kusunose, Y. Yanagi, Y. Motome, and H. Seo, Spin current generation in organic antiferromagnets, *Nat. Commun.* **10**, 4305 (2019).

[6] S. Hayami, Y. Yanagi, and H. Kusunose, Momentum-Dependent Spin Splitting by Collinear Antiferromagnetic Ordering, *J. Phys. Soc. Jpn.* **88**, 123702 (2019).

[7] K.-H. Ahn, A. Hariki, K.-W. Lee, and J. Kuneš, Antiferromagnetism in RuO₂ as d -wave Pomeranchuk instability, *Phys. Rev. B* **99**, 184432 (2019).

[8] S. Hayami, Y. Yanagi, and H. Kusunose, Spontaneous antisymmetric spin splitting in noncollinear antiferromagnets without spin-orbit coupling, *Phys. Rev. B* **101**, 220403(R) (2020).

[9] S. Hayami, Y. Yanagi, and H. Kusunose, Bottom-up design of spin-split and reshaped electronic band structures in antiferromagnets without spin-orbit coupling: Procedure on the basis of augmented multipoles, *Phys. Rev. B* **102**, 144441 (2020).

[10] L. Šmejkal, R. González-Hernández, T. Jungwirth, and J. Sinova, Crystal time-reversal symmetry breaking and spontaneous Hall effect in collinear antiferromagnets, *Sci. Adv.* **6**, eaaz8809 (2020).

[11] I. I. Mazin, Altermagnetism in MnTe: Origin, predicted manifestations, and routes to detwinning, *Phys. Rev. B* **107**, L100418 (2023).

[12] O. J. Amin, A. Dal Din, E. Golias, Y. Niu, A. Zakharov, S. C. Fromage, C. J. B. Fields, S. L. Heywood, R. B. Cousins, F. Maccherozzi, J. Krempaský, J. H. Dil, D. Kriegner, B. Kiraly, R. P. Campion, A. W. Rushforth, K. W. Edmonds, S. S. Dhesi, L. Šmejkal, T. Jungwirth,

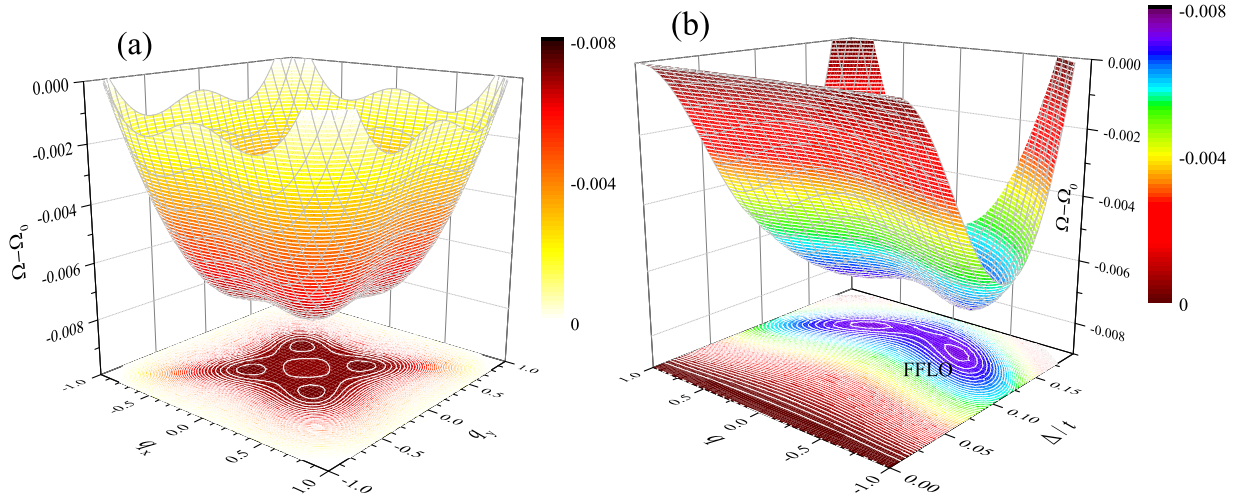


FIG. 11. (a) The landscape of the thermodynamic potential $(\Omega - \Omega_0)/(\nu t)$, as a function of the FFLO momenta q_x and q_y , at a pairing gap $\Delta_{\text{FFLO}} = 0.149t$. The thermodynamic potential reaches its minimum at $q_x = q_y = \pm q/\sqrt{2}$, the diagonal or off-diagonal direction. (b) The landscape of $(\Omega - \Omega_0)/(\nu t)$ as functions of the FFLO momenta $q = \pm \sqrt{q_x^2 + q_y^2}$ and the pairing gap Δ . In both plots, we have set the chemical potential $\mu_{\text{FFLO}} = 0.08t$. We consider the $d_{x^2-y^2}$ -wave altermagnetism with a coupling constant $t_{\text{am}} = 3.7t$, and take an attraction strength $U = -4t$. The filling factor of the lattice is $\nu = 0.03$.

and P. Wadley, Nanoscale imaging and control of altermagnetism in MnTe, *Nature* **636**, 348 (2024).

[13] V. S. de Carvalho and H. Freire, Unconventional superconductivity in altermagnets with spin-orbit coupling, *Phys. Rev. B* **110**, L220503 (2024).

[14] I. I. Mazin, Notes on altermagnetism and superconductivity, *AAPPS Bull.* **35**, 8 (2025).

[15] Y. Fukaya, B. Lu, K. Yada, Y. Tanaka, and J. Cayao, Superconducting phenomena in systems with unconventional magnets, *J. Phys.: Condens. Matter* **37**, 313003 (2025).

[16] S.-B. Zhang, L.-H. Hu, and T. Neupert, Finite-momentum Cooper pairing in proximitized altermagnets, *Nat. Commun.* **15**, 1801 (2024).

[17] P. Fulde and R. A. Ferrell, Superconductivity in a Strong Spin-Exchange Field, *Phys. Rev.* **135**, A550 (1964).

[18] A. I. Larkin and Yu. N. Ovchinnikov, Nonuniform state of superconductors, *Zh. Eksp. Teor. Fiz.* **47**, 1136 (1964) [Sov. Phys. JETP **20**, 762 (1965)].

[19] R. Casalbuoni and G. Nardulli, Inhomogeneous superconductivity in condensed matter and QCD, *Rev. Mod. Phys.* **76**, 263 (2004).

[20] S. Uji, T. Terashima, M. Nishimura, Y. Takahide, T. Konoike, K. Enomoto, H. Cui, H. Kobayashi, A. Kobayashi, H. Tanaka, M. Tokumoto, E. S. Choi, T. Tokumoto, D. Graf, and J. S. Brooks, Vortex Dynamics and the Fulde-Ferrell-Larkin-Ovchinnikov State in a Magnetic-Field-Induced Organic Superconductor, *Phys. Rev. Lett.* **97**, 157001 (2006).

[21] H. Hu and X.-J. Liu, Mean-field phase diagrams of imbalanced Fermi gases near a Feshbach resonance, *Phys. Rev. A* **73**, 051603(R) (2006).

[22] H. Hu, X.-J. Liu, and P. D. Drummond, Phase Diagram of a Strongly Interacting Polarized Fermi Gas in One Dimension, *Phys. Rev. Lett.* **98**, 070403 (2007).

[23] M. Kenzelmann, Th. Strässle, C. Niedermayer, M. Sigrist, B. Padmanabhan, M. Zolliker, A. D. Bianchi, R. Movshovich, E. D. Bauer, J. L. Sarrao, and J. D. Thompson, Coupled superconducting and magnetic order in CeCoIn₅, *Science* **321**, 1652 (2008).

[24] X.-J. Liu and H. Hu, Inhomogeneous Fulde-Ferrell superfluidity in spin-orbit-coupled atomic Fermi gases, *Phys. Rev. A* **87**, 051608(R) (2013).

[25] P. Wan, O. Zheliuk, N. F. Q. Yuan, X. Peng, L. Zhang, M. Liang, U. Zeitler, S. Wiedmann, N. E. Hussey, T. T. M. Palstra, and J. Ye, Orbital Fulde-Ferrell-Larkin-Ovchinnikov state in an Ising superconductor, *Nature* **619**, 46 (2023).

[26] D. Zhao, L. Debbeler, M. Kühne, S. Fecher, N. Gross, and J. Smet, Evidence of finite-momentum pairing in a centrosymmetric bilayer, *Nature Phys.* **19**, 1599 (2023).

[27] T. Kawamura and Y. Ohashi, Non-equilibrium BCS-BEC crossover and unconventional FFLO superfluid in a strongly interacting driven-dissipative Fermi gas, *AAPPS Bull.* **34**, 31 (2024).

[28] S. Sumita, M. Naka, and H. Seo, Fulde-Ferrell-Larkin-Ovchinnikov state induced by antiferromagnetic order in κ -type organic conductors, *Phys. Rev. Res.* **5**, 043171 (2023).

[29] D. Chakraborty and A. M. Black-Schaffer, Zero-field finite-momentum and field-induced superconductivity in altermagnets, *Phys. Rev. B* **110**, L060508 (2024).

[30] S. Hong, M. J. Park, and K.-M. Kim, Unconventional p -wave and finite-momentum superconductivity induced by altermagnetism through the formation of Bogoliubov Fermi surface, *Phys. Rev. B* **111**, 054501 (2025).

[31] I. V. Iorsh, Electron pairing by dispersive phonons in altermagnets: Reentrant superconductivity and continuous transition to finite momentum superconducting state, *Phys. Rev. B* **111**, L220503 (2025).

[32] G. Sim and J. Knolle, Pair Density Waves and Supercurrent Diode Effect in Altermagnets, *Phys. Rev. B* **112**, L020502 (2025).

[33] S. Sumita, M. Naka, and H. Seo, Phase-modulated superconductivity via altermagnetism, *Phys. Rev. B* **112**, 144510 (2025).

- [34] H. Hu, Z. Liu, and X.-J. Liu, Unconventional superconductivity of an altermagnetic metal: Polarized BCS and inhomogeneous FFLO states, *Phys. Rev. B* **112**, 184501 (2025).
- [35] K. Mukasa and Y. Masaki, Finite-momentum Superconductivity in Two-dimensional Altermagnets with a Rashba-type Spin-Orbit Coupling, *J. Phys. Soc. Jpn.* **94**, 064705 (2025).
- [36] Z. Liu, H. Hu, and X.-J. Liu, Fulde-Ferrell-Larkin-Ovchinnikov states and topological Bogoliubov Fermi surfaces in altermagnets: an analytical study, *arXiv:2508.07813* (2025).
- [37] R. Soto-Garrido and E. Fradkin, Pair-density-wave superconducting states and electronic liquid-crystal phases, *Phys. Rev. B* **89**, 165126 (2014).
- [38] A. T. Rømer, A. Kreisel, I. Eremin, M. A. Malakhov, T. A. Maier, P. J. Hirschfeld, and B. M. Andersen, Pairing symmetry of the one-band Hubbard model in the paramagnetic weak-coupling limit: A numerical RPA study, *Phys. Rev. B* **92**, 104505 (2015).
- [39] D. J. Thouless, Perturbation theory in statistical mechanics and the theory of superconductivity, *Ann. Phys. (N. Y.)* **10**, 553 (1960).
- [40] X.-J. Liu and H. Hu, BCS-BEC crossover in an asymmetric two-component Fermi gas, *Europhys. Lett.* **75**, 364 (2006).
- [41] R. D. Pisarski, V. V. Skokov, and A. M. Tsvelik, A pedagogical introduction to the Lifshitz regime, *Universe* **5**, 48 (2019).
- [42] H. Hu and X.-J. Liu, Quantum Lifshitz points in an altermagnetic superconductor, *AAPPS Bull.* **35**, 35 (2025).